



Transition Probabilities of Near-infrared Ce III Lines from Stellar Spectra: Applications to Kilonovae

Nanae Domoto¹, Jae-Joon Lee², Masaomi Tanaka^{1,3}, Ho-Gyu Lee^{2,4}, Wako Aoki^{5,6}, Miho N. Ishigaki⁵, Shinya Wanajo^{7,8}, Daiji Kato^{9,10}, and Kenta Hotokezaka^{11,12}

¹ Astronomical Institute, Tohoku University, Aoba, Sendai 980-8578, Japan; n.domoto@astr.tohoku.ac.jp

² Korea Astronomy and Space Science Institute, 776 Daedeok-daero, Yuseong-gu, Daejeon 34055, Republic of Korea

³ Division for the Establishment of Frontier Sciences, Organization for Advanced Studies, Tohoku University, Sendai 980-8577, Japan

⁴ Space Policy Research Center, Science and Technology Policy Institute, 370 Sicheong-daero, Sejong 30147, Republic of Korea

⁵ National Astronomical Observatory, 2-21-1 Osawa, Mitaka, Tokyo 181-8588, Japan

⁶ Astronomical Science Program, The Graduate University for Advanced Studies, SOKENDAI, 2-21-1 Osawa, Mitaka, Tokyo 181-8588, Japan

⁷ Max-Planck-Institut für Gravitationsphysik (Albert-Einstein-Institut), Am Mühlenberg 1, D-14476 Potsdam-Golm, Germany

⁸ Interdisciplinary Theoretical and Mathematical Sciences Program (iTHEMS), RIKEN, Wako, Saitama 351-0198, Japan

⁹ National Institute for Fusion Science, 322-6 Oroshi-cho, Toki 509-5292, Japan

¹⁰ Interdisciplinary Graduate School of Engineering Sciences, Kyushu University, Kasuga, Fukuoka 816-8580, Japan

¹¹ Research Center for the Early Universe, Graduate School of Science, University of Tokyo, Bunkyo, Tokyo 113-0033, Japan

¹² Kavli IPMU (WPI), UTIAS, The University of Tokyo, Kashiwa, Chiba 277-8583, Japan

Received 2023 June 30; revised 2023 August 31; accepted 2023 September 1; published 2023 October 13

Abstract

Kilonova spectra provide us with information of r -process nucleosynthesis in neutron star mergers. However, it is still challenging to identify individual elements in the spectra mainly due to the lack of experimentally accurate atomic data for heavy elements at near-infrared wavelengths. Recently, Domoto et al. proposed that the absorption features around 14500 Å in the observed spectra of GW170817/AT2017gfo are Ce III lines. But they used theoretical transition probabilities (gf -values) whose accuracy is uncertain. In this paper, we derive the astrophysical gf -values of three Ce III lines, aiming at verifying this identification. We model high-resolution H -band spectra of four F-type supergiants showing clear Ce III absorption features by assuming stellar parameters derived from optical spectra in the literature. We also test the validity of the derived astrophysical gf -values by estimating the Ce III abundances of Ap stars. We find that the derived astrophysical gf -values of the Ce III lines are systematically lower by about 0.25 dex than those used in previous work of kilonovae, while they are still compatible within the uncertainty ranges. By performing radiative transfer simulations of kilonovae with the derived gf -values, we find that the identification of Ce III as a source of absorption features in the observed kilonova spectra still stands, even considering the uncertainties in the astrophysical gf -values. This supports the identification of Ce in the spectra of GW170817/AT2017gfo.

Unified Astronomy Thesaurus concepts: R-process (1324); Radiative transfer simulations (1967); Transition probabilities (2074)

1. Introduction

Binary neutron star (NS) mergers have been considered as promising sites of r -process nucleosynthesis (e.g., Eichler et al. 1989; Freiburghaus et al. 1999; Goriely et al. 2011; Korobkin et al. 2012; Wanajo et al. 2014). In 2017, associated with the detection of gravitational waves (GWs) from a NS merger (GW170817; Abbott et al. 2017a), the electromagnetic counterpart AT2017gfo was observed (Abbott et al. 2017b). The observed properties of AT2017gfo at ultraviolet, optical, and near-infrared (NIR) wavelengths are consistent with the theoretical expectation of a kilonova (Li & Paczyński 1998; Metzger et al. 2010), thermal emission from NS merger ejecta powered by the radioactive decay of r -process nuclei (e.g., Arcavi et al. 2017; Evans et al. 2017; Pian et al. 2017; Smartt et al. 2017; Utsumi et al. 2017; Valenti et al. 2017). This electromagnetic counterpart has provided us with evidence that NS mergers are sites of r -process nucleosynthesis (e.g., Kasen et al. 2017; Perego et al. 2017; Shibata et al. 2017;

Tanaka et al. 2017; Kawaguchi et al. 2018; Rosswog et al. 2018).

To extract detailed information of the elements synthesized in NS merger ejecta, it is important to identify the individual elements. However, element identification in kilonova spectra remains challenging. This is mainly due to the lack of atomic data for heavy elements. While detailed spectral studies require spectroscopically accurate atomic data, such data for heavy elements have been highly incomplete, especially at NIR wavelengths. So far, the absorption features around 8000 Å in the photospheric spectra of AT2017gfo have been identified as Sr II (Watson et al. 2019; Domoto et al. 2021; Gillanders et al. 2022), although the same features may be caused by He I (Perego et al. 2017; Tarumi et al. 2023).

Recently, Domoto et al. (2022) systematically studied kilonova spectra over the entire wavelength range. They identified important elements that produce strong transitions in kilonovae, such as Ca, Sr, Y, Zr, Ba, La, and Ce. Then, they constructed a hybrid line list combined with experimentally accurate data for important elements and complete theoretical data for weak transitions of the other elements (Tanaka et al. 2020). By performing radiative transfer simulations, they found that the broad-line features at ~ 13000 and 14500 Å in the

spectra of AT2017gfo can be explained by La III and Ce III, respectively. However, this identification can be still a subject of discussion as they adopted the transition probabilities (i.e., gf -values) of the La III and Ce III lines from theoretical calculations (Tanaka et al. 2020) due to a lack of experimental measurements.

The lack of experimental atomic data is problematic in any spectra for astrophysical objects, such as stars. Compared with the optical region, line identification in stellar spectra in the NIR region is incomplete and still in progress (e.g., Matsunaga et al. 2020). Also, as few experiments have been performed on heavy elements such as lanthanides, gf -values from theoretical calculations are commonly used even for optical wavelengths. In many cases, no or few data are provided for NIR wavelengths (e.g., Biémont et al. 1999; Quinet & Palmeri 2020).

In general, the accuracy of atomic calculations is difficult to assess without experimental measurements. It has been shown that the theoretical gf -values for given ions differ from the experimental values by factors up to several for strong transitions, and even more for weak transitions (see, e.g., the appendix of Domoto et al. 2022). The gf -values directly affect the absorption depths in the spectra, which influence the derived parameters, e.g., abundances. In the case of the kilonova model of Domoto et al. (2022), the absorption features at the NIR wavelengths can disappear if the gf -values of the NIR lines are ~ 10 times smaller than the values they adopted. Therefore, it is important to measure the gf -values to identify elements in kilonova spectra firmly.

For their use in astrophysics, one can estimate the gf -values of atomic lines by using stellar spectra. These are often called “astrophysical gf -values.” Such work has been performed for many metal lines at NIR wavelengths using the spectra of well-observed stars, e.g., the Sun (e.g., Meléndez & Barbuy 1999). In fact, it has been shown that astrophysical gf -values can be useful to extract elemental information from stars without laboratory experiments (Hasselquist et al. 2016; Cunha et al. 2017).

In this paper, we derive the astrophysical gf -values of three Ce III lines in the H band (around $1.6 \mu\text{m}$) using high-resolution stellar spectra. We aim to verify the identification of Ce in the spectra of AT2017gfo. Note that we cannot test the absorption by La III in the same way, because the La III lines at rest lie in the wavelength region of strong atmospheric absorption. In Section 2, we describe the targeted Ce III lines in more detail. We present stellar spectra showing Ce III line features in Section 3, and derive the gf -values of the Ce III lines by modeling these spectra in Section 4. In Section 5, we apply the derived gf -values of the Ce III lines to kilonova spectra by performing radiative transfer simulations. Finally, we give a summary in Section 6. We also show the validity of our results by estimating the Ce abundances with Ce III lines in Ap stars in Appendix. Throughout of the paper, line wavelengths are written as those in a vacuum unless otherwise mentioned.

2. Ce III lines in the H band

We focus on the three Ce III lines in the H band (Table 1). It has been shown that these are the strongest lines of Ce III in the NIR region, which can produce broad absorption features in kilonova spectra (Domoto et al. 2022). In fact, these lines have been detected in the spectra of Ap/Bp stars that exhibit

enhanced Ce abundances (Hubrig et al. 2012; Chojnowski et al. 2019; Tanaka et al. 2023).

Although the transition wavelengths of these lines have been measured by experiments (Johansson & Litzén 1972), their transition probabilities are experimentally unknown. Thus, Domoto et al. (2022) adopted the theoretical results of Tanaka et al. (2020). Other theoretical calculations are also available, i.e., used for studies of optical stellar spectra (Wyart & Palmeri 1998; Biémont et al. 2002) and for application to kilonovae (Carvajal Gallego et al. 2021). However, it is usually difficult to assess the accuracy of these calculations, and the gf -values vary over the range of ~ 0.5 dex as shown in Table 1.

Recently, the APOGEE survey has observed many Galactic stars in the H band with a spectral resolution of $R \sim 22,500$ (Majewski et al. 2017). To analyze the APOGEE spectra, line lists for the H band have been provided (Shetrone et al. 2015; Holtzman et al. 2018; Smith et al. 2021). These authors collected atomic data from theoretical and experimental studies, and adjusted the gf -values by fitting those to the spectra of the Sun and Arcturus. It was shown that such astrophysical gf -values can improve agreement between observed spectra and model spectra. In fact, the APOGEE line lists include the three Ce III lines on which we focus (Table 1). However, their astrophysical gf -values are quite uncertain, because there is no clear Ce III absorption in the spectra of the Sun and Arcturus. As a result, the gf -values vary by an order of magnitude across the different versions of the APOGEE line lists. This fact demonstrates that, if lines are not clearly detected in the spectra, which is the case of the Ce III lines for the Sun and Arcturus, it is difficult to derive their astrophysical gf -values even though the spectra are well characterized. To derive the gf -values of the Ce III lines, we select stars clearly showing these Ce III line features (Section 3), although the uncertainties in the stellar parameters can be larger than those of well-known stars such as the Sun and Arcturus (Section 4.3).

We mention that near the three lines, there is another Ce III line at 15964.93 \AA . According to the theoretical gf -values of this line (-1.272 by Tanaka et al. 2020; -1.660 by Biémont et al. 2002; see Chojnowski et al. 2019; and -1.690 by Carvajal Gallego et al. 2021), this line is weaker than the three Ce III lines. In fact, it is found that the absorption at this wavelength is usually dominated by the strong Si I $\lambda 15964.41$ line (see Figure 1). Thus, we will not focus on this line in this work.

3. Stellar Spectra with Ce III Lines

3.1. Sample Selection

Compared with NIR wavelengths, the line list in the optical region is more comprehensive and accurate. Ce abundances in many stars are indeed reported from optical observations, e.g., in the Hypatia Catalog in the solar neighborhood (Hinkel et al. 2014), a catalog of luminous stars (Luck 2014), and a catalog of chemically peculiar (CP) stars (Ghazaryan et al. 2018). While not all of the stars in these catalogs have Ce abundances, measurements are available for a good fraction of them. Thus, we will derive the astrophysical gf -values of the Ce III lines using stars that (1) show Ce III line features in the NIR H band and (2) have known Ce abundances from optical spectra.

We obtain NIR H -band high-resolution spectra from the spectral archive of the Immersion GRating INfrared Spectrometer (IGRINS; Park et al. 2014; Mace et al. 2016, 2018).

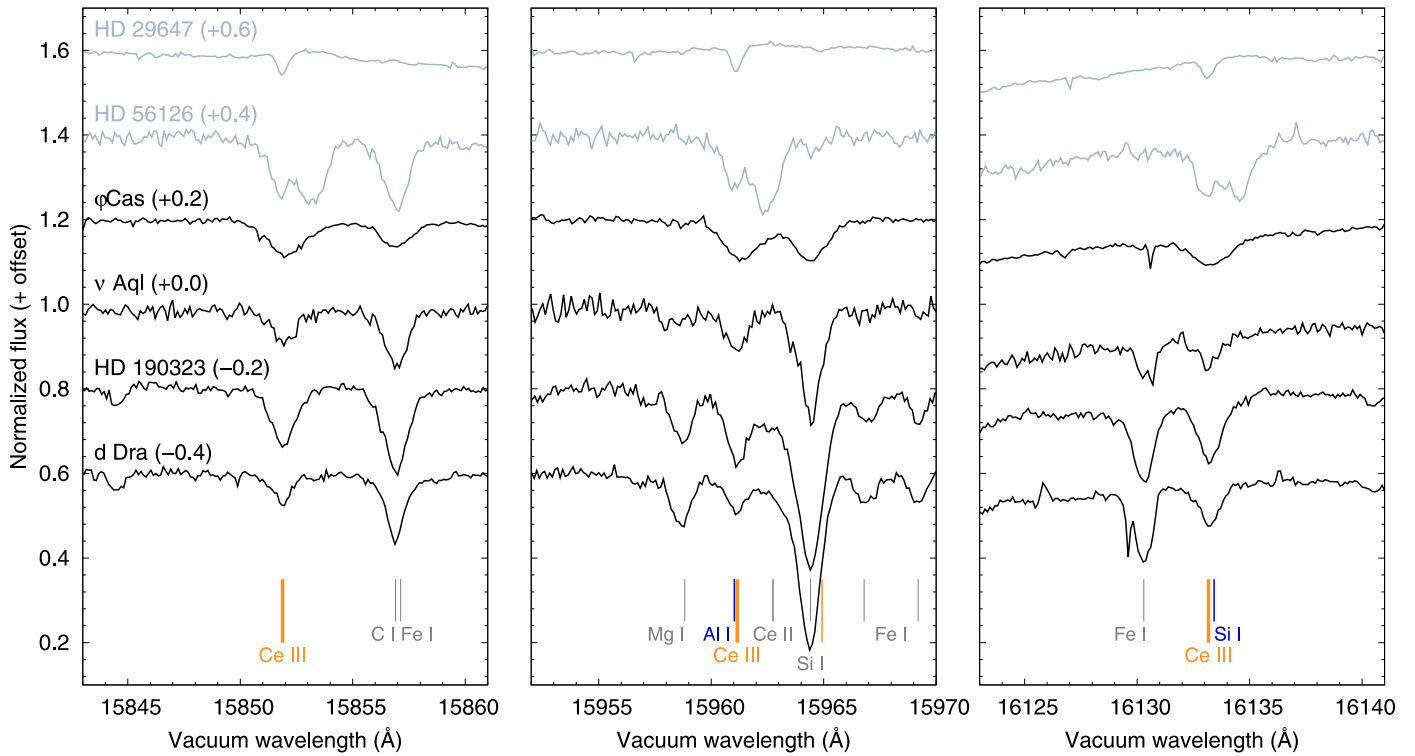


Figure 1. The IGRINS spectra around the Ce III lines of the selected stars. Black and gray lines show the spectra for the objects used as the final sample and for the excluded objects, respectively (see the text). The positions of the three Ce III lines that we focus on are indicated by thick orange lines (Table 1), while that of another Ce III line is also indicated by a thin orange line (see Section 2). Al I and Si I lines that may contaminate the Ce III lines are labeled in blue. Other lines are also shown in gray.

Table 1
The Targeted Ce III Lines in the *H* band

λ_{vac}^a (Å)	λ_{air}^b (Å)	E_{lower}^c (cm^{-1})	E_{upper}^d (cm^{-1})	Theoretical $\log gf^e$				Astrophysical $\log gf^f$			
				(1)	(2)	(3)	(4)	(5)	(6)	(7)	This work
15851.880	15847.550	1528.32	7836.72	-0.613	-0.838	-1.030	-1.190	-0.439	-0.673	-2.105	-0.861
15961.157	15956.797	0.00	6265.21	-0.721	-0.926	-1.120	-1.290	-2.926	-1.098	-0.345	-0.966
16133.170	16128.763	3127.10	9325.51	-0.509	-0.722	-0.920	-1.070	-0.429	-1.950	-0.920	-0.702

Notes.

^a Vacuum transition wavelength.

^b Air transition wavelength.

^c Lower energy level.

^d Upper energy level.

^e gf -values from theoretical calculations: (1) Tanaka et al. (2020); see also Domoto et al. (2022); (2) Wyart & Palmeri (1998); (3) taken from Hubrig et al. (2012) and Chojnowski et al. (2019). These values were computed in the same way as in Biémont et al. (2002) and provided to Hubrig et al. (2012) and Chojnowski et al. (2019) in private communications; and (4) Carvajal Gallego et al. (2021). For (1) and (4), theoretical gf -values are shown as they are, without calibration by considering the differences in the theoretical energy levels relative to the experimental energy levels.

^f Astrophysical gf -values in the APOGEE line list: (5) Table 7 of Shetrone et al. (2015); (6) taken from here through the Sloan Digital Sky Survey (SDSS) Science Archival Server (SAS), see Holtzman et al. (2018); (7) taken from here through the SDSS SAS, see Smith et al. (2021); and those derived in this work (Section 4).

IGRINS provides spectra spanning the full *H* and *K* bands with a spectral resolution of $R \sim 45,000$. The Raw & Reduced IGRINS Spectral Archive (RRISA)¹³ contains the IGRINS archive for the period 2014 July–2021 December, containing data from the 2.7 m Harlan J. Smith Telescope at McDonald Observatory, the Discovery Channel Telescope at Lowell Observatory, and the Gemini-South telescope. RRISA includes IGRINS data from more than 850 nights on sky, resulting in 2800 unique target observations from over 3000 hr of the total

science time. RRISA also includes IGRINS observations of >1200 distinct AOV standard stars.

RRISA provides reduced one-dimensional (1D) spectra processed using the IGRINS pipeline (Lee et al. 2017). The pipeline applies flat fielding and flagging of bad pixels, and the 1D spectra are extracted using the optimal extraction of Horne (1986). The wavelength solutions are derived using OH lines from sky spectra. In the *H* band, the accuracy of the wavelength solution is better than 0.01 \AA ($\sim 0.2 \text{ km s}^{-1}$). RRISA further refines the wavelength of the pipeline product by improving the pixel alignment between the AOV star spectrum and the target spectrum using strong telluric sky lines between

¹³ <https://igrinscontact.github.io/>

Table 2
Adopted Stellar Parameters for the Sample of Stars

Star	Spectral type	Model	T_{eff} (K)	$\log g$ (cm s^{-2})	[Fe/H]	ξ (km s^{-1})	$v \sin i$ (km s^{-1})	[Al/H]	[Si/H]	[Ce/H]	$\sigma_{\text{[Ce/H]}}^a$
φ Cas	F0Ia	ATLAS	7347	0.76	-0.07	5.21	23.0*	0.00 ^b	0.49	0.16	0.30
ν Aql	F2Ib	ATLAS	7152	1.65	0.10	3.74	12.0**	0.22	0.32	0.27	0.22
HD 190323	F8Ia	MARCS	6169	1.11	0.12	4.31	15.0 [‡]	0.42	0.27	0.25	0.15
d Dra	F8Ib-2	MARCS	6157	1.78	-0.10	3.93	10.0 [†]	0.16	0.06	0.27	0.24

Notes. All parameters are adopted from Luck (2014), except $v \sin i$ from Abt & Morrell (1995; *), Uesugi & Fukuda (1970; **), Lyubimkov et al. (2012; †), and estimated in this work using the Ce III line because of no available measurements (‡).

^a Standard deviations of the Ce abundances measured in Luck (2014; see Section 4.3).

^b Solar abundance (Asplund et al. 2009) is assumed because it is not measured in Luck (2014).

16452–16458 Å and 21740–21752 Å in the *H* and *K* bands, respectively. Telluric absorption is corrected using the spectra of A0V stars observed closely in time and airmass, with the intrinsic features of A0V stars removed using a model spectrum of Vega (Castelli & Kurucz 1994).

We cross-match the RRISA archive with two stellar catalogs of measured abundances: Luck (2014) and Ghazaryan et al. (2018). Not all entries in these catalogs have Ce abundances reported, and they are not used as we need abundance information to derive the *gf*-values (see below). Luck (2014) reports abundances for 451 luminous stars including Ce measurement for 448 stars. RRISA contains spectra for 27 of them. Ghazaryan et al. (2018) reports abundances of 429 CP stars with 121 stars having Ce measurements. RRISA contains the spectra of eight stars.

For the matched data, we apply Doppler corrections using strong C I, Si I, and Fe I lines. Then, we visually check the absorption lines at the wavelengths of the Ce III lines. We impose the detection of all three lines to ensure the origin of these lines. As a result, six stars showing clear Ce III line features are selected: HD 29647, HD 56126, φ Cas, ν Aql, HD 190323, and d Dra. The spectra of these six stars around the region of the Ce III lines are shown in Figure 1.

While the six stars are selected above, we decide not to use two of them: HD 29647 and HD 56126 (gray lines in Figure 1). This is because their atmospheric parameters are found to be rather uncertain, although they are listed in the catalogs. For HD 29647, an HgMn star (Straizys et al. 1985), Adelman et al. (2001) have reported atmospheric parameters, but they mentioned that the parameters are not very accurate. For HD 56126, a post-AGB star (e.g., Hony et al. 2003), its atmospheric parameters seem to change depending on the epoch when the spectra were taken (De Smedt et al. 2016; Puķītis 2022). Puķītis (2022) also pointed out the chemical depletion of neutron-capture elements in other post-AGB stars, likely due to dust condensation. Also, the IGRINS spectrum of HD 56126 shows double-peaked features, whose origins are unknown.

Finally, we use four stars as our sample (black lines in Figure 1). The signal-to-noise ratios (S/Ns) of the spectra around the targeted Ce III lines are >100 for ν Aql and >200 for the others. Since the Ce III $\lambda 15851.88$ and $\lambda 16133.170$ lines are located around broad hydrogen features, the spectra are normalized by fitting the broad features as a pseudocontinuum. After the normalization, we measure the equivalent widths (EWs) of the Ce III lines by Gaussian fitting (see the top panels of Figure 3 as examples). The measured EWs of the Ce III lines

in each star are shown in Table 3, which are used to derive the astrophysical *gf*-values in Section 4.

3.2. Properties of the Sample Stars

The four stars in our final sample are all F-type supergiants (see Table 2). The primary catalog of Luck (2014) consists primarily of (super)giants with $T_{\text{eff}} \sim 4000$ –8000 K, and the Ce III lines are only seen in warmer supergiants of $T_{\text{eff}} > 6000$ K. To check for the presence of the Ce III lines in wider parameter ranges of T_{eff} and surface gravity $\log g$, we also cross-matched the RRISA with Hinkel et al. (2014). The RRISA contains spectra of 132 sources out of 2685 stars from Hinkel et al. (2014), primarily of nearby dwarf stars. But none of the spectra show a clear signature of the Ce III lines. We further check the RRISA with the T_{eff} and $\log g$ from the PASTEL catalog (Soubiran et al. 2016). The RRISA contains spectra of 168 stars with $T_{\text{eff}} \sim 5500$ –8000 K, mostly dwarfs with some (super)giants. Note that this catalog does not provide abundance measurements and is not subject to our analysis of deriving the *gf*-values. We find five stars showing the Ce III line features, which are the same four stars as our sample selected from Luck (2014) and an additional F-type supergiant.

We briefly discuss the reason why the Ce III lines tend to appear in warm supergiants. To see the behavior of the Ce III absorption in spectra, we generate model spectra for the wavelength regions around the Ce III lines, varying T_{eff} and $\log g$. We use Turbospectrum (Plez 2012) implemented through iSpec (Blanco-Cuaresma et al. 2014; Blanco-Cuaresma 2019) to perform the spectral synthesis, assuming local thermodynamic equilibrium (LTE). The parameter ranges are $T_{\text{eff}} = 5000$ –10,000 K and $\log g = 0.5$ –4.5 dex with intervals of 500 K and 0.5 dex, respectively. For simplicity, we fix the microturbulence velocity $\xi = 2 \text{ km s}^{-1}$, the solar abundance ratio (Asplund et al. 2009), and the projected rotational velocity $v \sin i = 10 \text{ km s}^{-1}$ as typical values (e.g., Matsunaga et al. 2020), and assume a macroturbulence velocity $v_{\text{mac}} = 0 \text{ km s}^{-1}$ (see also Section 4.1). We use ATLAS, a 1D plane-parallel atmosphere model (Castelli & Kurucz 2003). For the atomic data, we use the APOGEE line list (Holtzman et al. 2018; Smith et al. 2021; see Section 4.1) as a baseline, with the line list of the Ce III lines from Domoto et al. (2022). These choices do not affect the dependence on T_{eff} and $\log g$ discussed here.

Since the dependence of the absorption on the atmospheric parameters is expected to be the same among the Ce III lines, we focus only on the Ce III $\lambda 15961.157$ line. Note that this Ce III line may be contaminated by the Al I $\lambda 15961.03$ line at lower T_{eff} and higher $\log g$, although the Ce III line is dominant (Section 4.1). We measure the EWs of the Ce III line in the

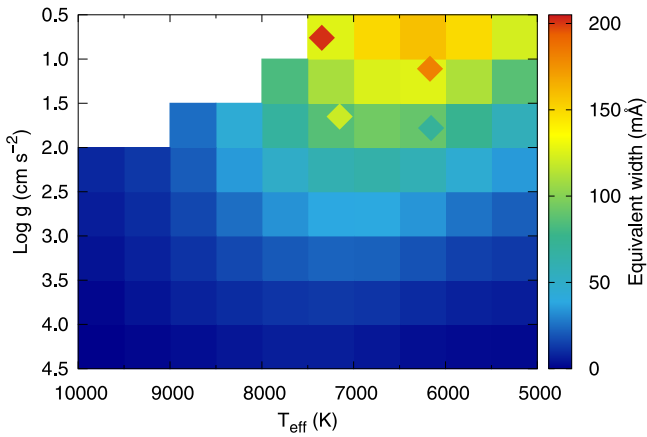


Figure 2. EW of the Ce III $\lambda 15961.157$ line in the model spectra (colormap) and in the observed spectra (diamonds). Note that the region without color (upper left) is the parameter space where no ATLAS model exists.

model spectra by Gaussian fitting as done for the observed spectra. The measured EWs for different T_{eff} and $\log g$ are shown in Figure 2. It is seen that the EW of the Ce III line peaks at $T_{\text{eff}} \sim 6000\text{--}7000$ K and $\log g < 2$. The peak T_{eff} can be understood as the region where the doubly ionized Ce is the most abundant under LTE. Also, the line becomes strong toward low gravity, due to the low-density and geometrically thick atmosphere (Gray 2005). A similar trend is observed for other lines of metal ions (Matsunaga et al. 2020).

We also show the observed EW of the Ce III $\lambda 15961.157$ line for the four sample stars with diamonds in Figure 2. Although the Ce abundances are not exactly the same as the solar abundances for these stars, it is seen that the observed trend is consistent with the trend in our model grid. Also, the models are consistent with the fact that only warm (F-type) supergiants show Ce III lines and not normal dwarfs.

Of course, the behavior of the Ce III lines is also dependent on the Ce abundance. If the Ce abundance is higher, the parameter ranges of T_{eff} and $\log g$ showing the Ce III lines become wider. For example, as shown in Figure 1, HD 29647 shows Ce III absorption at NIR wavelengths even under high temperature and strong surface gravity ($T_{\text{eff}} \sim 12,500$ K and $\log g \sim 4$; Adelman et al. 2001), because the Ce abundance is ~ 3 dex higher than the solar value (see also Appendix). We note that CP stars are main-sequence stars; the supergiants used in our analysis do not show such anomaly in the abundances of lanthanides.

4. Astrophysical gf -values of the Ce III Lines

4.1. Methods

In this section, we derive the astrophysical gf -values of the Ce III lines. For each sample star, we perform spectral synthesis calculations with the fixed Ce abundances based on the measurements with the optical spectra, and then adjust the gf -values. We use Turbospectrum (Plez 2012) through iSpec (Blanco-Cuaresma et al. 2014; Blanco-Cuaresma 2019) to synthesize spectra as in Section 3.2.

We adopt atmospheric parameters (T_{eff} , $\log g$, metallicity, and ξ) derived from the analysis of optical spectra. Luck (2014) provided the stellar parameters of sample stars using MARCS models (Gustafsson et al. 2008). For stars with T_{eff} higher than ~ 6300 K, they also used ATLAS models (Castelli & Kurucz 2003). In our sample, when a star has two parameter

sets determined using both models, we use the atmospheric parameters that better reproduce the H -band IGRINS spectra. Then, for spectral synthesis, we consistently use the MARCS or ATLAS models used in the estimates of the adopted atmospheric parameters. The adopted atmospheric parameters and models of sample stars are summarized in Table 2.

We use the elemental abundances derived using the adopted atmospheric parameters in Luck (2014). Luck (2014) used observational data from multiple archives and provided abundances for each of the available data sets for a given star. When multiple abundance sets are provided for our sample stars, we simply take the average. While all the elements are included in our calculations, only Ce, Al, and Si are important for our analysis: Ce abundances directly affect the absorption depths of the Ce III lines, while Al and Si may also affect the Ce III absorption due to contamination by the Al I $\lambda 15961.03$ and Si I $\lambda 16133.42$ lines, respectively. For elements without measurements, we assume solar abundances (Asplund et al. 2009). For example, the Al abundance for φ Cas is assumed as solar. But this assumption does not affect the results because most Al is expected to be ionized in a high T_{eff} (~ 7300 K) and low $\log g$ (~ 0.8 dex) atmosphere (see also Section 4.3 and Table 4). For all the samples, the contamination from the Al I and Si I lines for the Ce III absorption features is estimated to be $< 10\%$ and $< 30\%$, respectively, by measuring the EWs of the lines in the model spectra without Ce III lines. The adopted abundances of the important elements are also summarized in Table 2.

It should be cautioned that, although the Ce abundances are fixed in our analysis, they are also subject to uncertainties (see also Section 4.3). The standard deviations of the Ce abundances measured in Luck (2014) are also shown in Table 2. We confirmed that the absorption of Ce II lines at the H band (Cunha et al. 2017) is reasonably reproduced for HD 190323 and d Dra, which confirms the validity of the abundances. There is no or little Ce III absorption for φ Cas and ν Aql with $T_{\text{eff}} > 7000$ K. Nevertheless, we emphasize that the Ce abundances in these two stars are rather robust, because they were derived using optical lines with experimental gf -values (Luck 2014).

Spectral synthesis also needs to consider the effects of line broadening. It is usually difficult to separate the effects of $\nu \sin i$ and v_{mac} on the line profiles of F-type supergiants (e.g., Lyubimkov et al. 2012). Here, we ignore v_{mac} and consider only $\nu \sin i$. These parameters for φ Cas, ν Aql, and d Dra are taken from the literature (see Table 2). We find that these choices reasonably reproduce the line profiles in the IGRINS spectra. On the other hand, no measurement of $\nu \sin i$ for HD 190323 was found. Thus, we estimate $\nu \sin i$ using the Ce III lines in the IGRINS spectra (see Table 2). Although this is not a very accurate measurement, this assumption does not affect our results.

The line list for other elements is also an important factor in the estimate of gf -values. This is because some Ce III lines are contaminated by Al I or Si I lines. Thus, the gf -values of these lines may affect the estimates of the gf -values of the Ce III lines. By comparing the H -band model spectra using the VALD (Piskunov et al. 1995; Kupka et al. 1999; Ryabchikova et al. 2015) and the APOGEE line lists (Holtzman et al. 2018; Smith et al. 2021), we find that the APOGEE line list reproduces the observed features of the IGRINS spectra better. Thus, we adopt the APOGEE line list for our analysis. Note

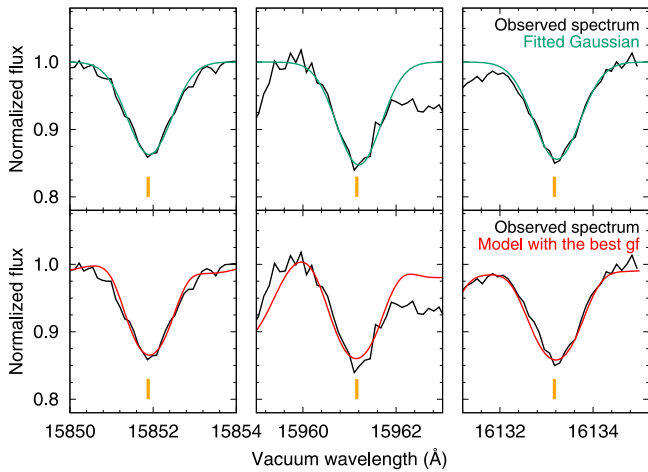


Figure 3. The Ce III lines of HD 190323 (black). In the top panels, the observed spectra are compared with the fitted Gaussian profile (green). In the bottom panels, the observed spectra are compared with the model spectra using the derived gf -values (red). Note that the observed spectrum at ~ 15963 Å of HD 190323 (the middle panels) may be affected by unknown lines.

that, as iSpec implements the APOGEE line list of DR13/14 (Holtzman et al. 2018), we updated the line list using the newest DR16 line list (Smith et al. 2021) except for hyperfine structure lines.

For the model spectra, we measure the EWs of the Ce III lines by Gaussian fitting as done for the observed spectra. These EWs are compared with those of the observed spectra (Section 3.1). Comparison is repeated by changing the gf -values of the Ce III lines. Finally, we adopt the gf -values that give the EWs best in agreement with the EWs of the observed spectra. Examples of the final model spectra are shown in the bottom panels of Figure 3.

4.2. Results

The estimated gf -values of the three Ce III lines using the spectra of the four stars are shown by blue dots in Figure 4, and listed in Table 3. As our final astrophysical gf -value of each Ce III line, we take the averages of those derived for each star. They are plotted as red dots in each panel of Figure 4, and listed in Table 1. The validity of our final gf -values is also discussed in Appendix.

The gf -values of the Ce III lines from available theoretical calculations are also shown by black diamonds in Figure 4 (see Table 1). All of our gf -values are consistently smaller than those of Tanaka et al. (2020), which were used for the kilonova model of Domoto et al. (2022). This suggests that the strength of absorption could have been overestimated in the kilonova model of Domoto et al. (2022; see Section 5). On the other hand, it is seen that the estimated final gf -values are the closest to those of Wyart & Palmeri (1998), while higher than those of Biémont et al. (2002) and Carvajal Gallego et al. (2021). Overall, our gf -values of the Ce III lines, which are independently estimated from theoretical calculations, broadly agree with the available theoretical calculations within the margin of the estimated uncertainties discussed in Section 4.3.

4.3. Uncertainties in the gf -values

Uncertainties in the astrophysical gf -values can be evaluated by considering the uncertainties in the stellar parameters of each star. The systematic uncertainties of stellar parameters can

Table 3
Observed EWs and Derived gf -values for the Three Ce III Lines in the Four Sample Stars

Star	EW	$\log gf$	EW	$\log gf$	EW	$\log gf$
	(mÅ)		(mÅ)		(mÅ)	
	15851.880 Å		15961.157 Å		16133.170 Å	
φ Cas	184	-0.82	201	-0.80	166	-0.72
ν Aql	102	-0.93	120	-0.96	96	-0.83
HD 190323	183	-0.78	182	-0.90	180	-0.65
d Dra	81	-0.92	71	-1.20	113	-0.61

generally be caused by differences in the analysis methods. Even with common atmospheric parameters and line lists, there remain variety in the abundances determined by different codes and methods (Hinkel et al. 2016) as well as the different spectral data used in the analysis (Luck 2014). All of these factors can affect the depth of the absorption lines, which leads to uncertainties in the astrophysical gf -values derived for the fixed Ce abundances.

We estimate the systematic uncertainties in our astrophysical gf -values by varying the stellar parameters of each star. To take the uncertainties of the stellar parameters into account, we vary T_{eff} by ± 200 K, $\log g$ by ± 0.3 dex, $[\text{Fe}/\text{H}]$ by ± 0.3 dex, and ξ by ± 0.5 km s $^{-1}$. Also, we vary $[\text{Al}/\text{H}]$ and $[\text{Si}/\text{H}]$ by ± 0.5 and ± 0.3 dex, respectively, which affect the level of the contamination. These ranges are the typical systematic uncertainties caused by the different codes and methods used to determine the stellar parameters (Hinkel et al. 2016). While Hinkel et al. (2016) used dwarfs to show these uncertainty ranges, the uncertainties for supergiants are similar to those in dwarfs (Luck 2014).

Table 4 summarizes the estimated systematic uncertainties in the astrophysical gf -values of the Ce III lines. Only the results for the positive shifts are shown, but the results for the negative shifts are smaller than the uncertainties given in Table 4 (see also Table 3 of Cunha et al. 2017). We find that the largest uncertainties are caused by T_{eff} and $\log g$. The systematic uncertainties in total in each gf -value for each star (Δ_{sys}) are estimated by taking the root sum square (Cunha et al. 2017). Note that the values of Δ_{sys} estimated here are the upper limits of the uncertainties; all the stellar parameters are not independent, and the uncertainties caused by each parameter may be canceled among parameters (Cunha et al. 2017). In most cases, the total systematic uncertainties are smaller than 0.2 dex, and up to ~ 0.26 dex. These systematic uncertainties are shown as the error bars on the blue dots in Figure 4.

Finally, we assign the systematic uncertainties of the average astrophysical gf -values by taking rms of the Δ_{sys} for the four stars. The systematic uncertainties in the gf -values for the $\lambda 15851.880$, $\lambda 15961.157$, and $\lambda 16133.170$ lines are 0.182, 0.186, and 0.213, respectively (shown as the error bars on the red dots in Figure 4). It is worth noting that our astrophysical gf -values broadly agree with available theoretical calculations, considering the systematic uncertainties.

Here we did not show the uncertainties in the continuum levels of the observed spectra in Δ_{sys} . They may affect the observed EWs and in turn the astrophysical gf -values. However, the uncertainties in the continuum levels and their contributions to Δ_{sys} are estimated to be $\lesssim 1\%$, which are smaller than the uncertainties from most stellar parameters (see also Table 3 of Cunha et al. 2017).

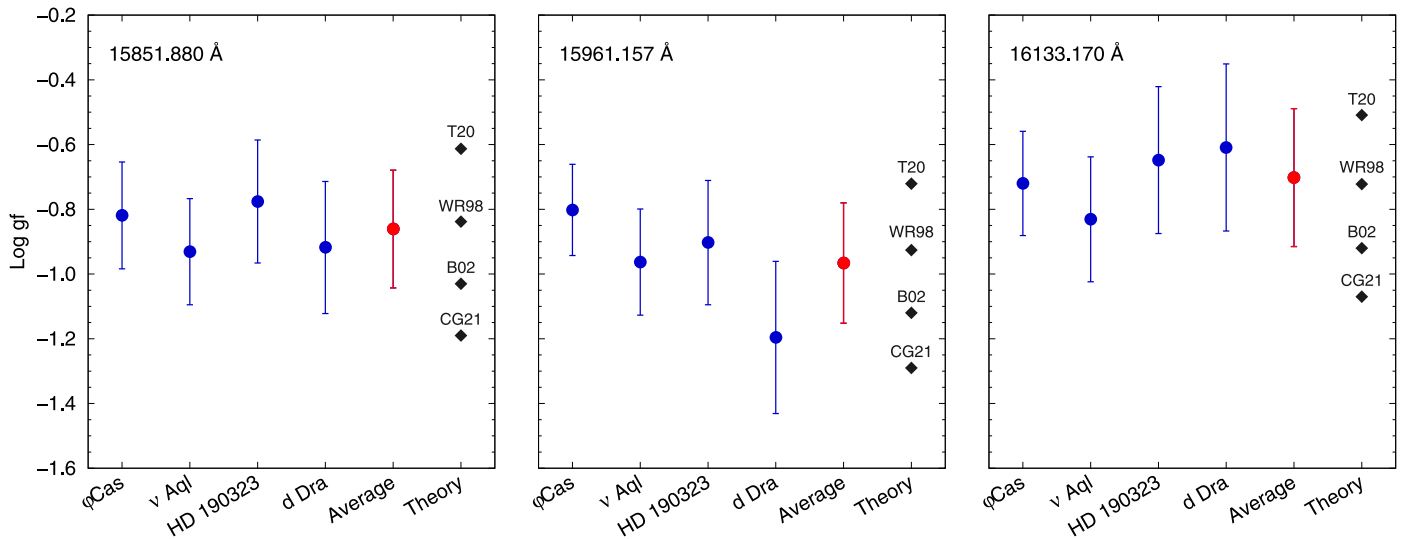


Figure 4. Astrophysical gf -values of the Ce III lines derived from four stellar spectra (blue dots), and their average (red dots). Each panel shows the results of each transition as shown in the legend. Black diamonds show the theoretical gf -values (T20: Tanaka et al. 2020; WR98: Wyart & Palmeri 1998; B02: Biémont et al. 2002, see Table 1; CG21: Carvajal Gallego et al. 2021). Error bars indicate the estimated systematic uncertainties (see Section 4.3 and Table 4).

Table 4
Systematic Uncertainties in the Astrophysical gf -values of the Ce III Lines for the Fixed Ce Abundances in Each Star

Star	λ_{vac} (Å)	ΔT_{eff} (+200 K)	$\Delta \log g$ (+0.3 dex)	$\Delta[\text{Fe}/\text{H}]$ (+0.3 dex)	$\Delta \xi$ (+0.5 km s ⁻¹)	$\Delta[\text{Al}/\text{H}]$ (+0.5 dex)	$\Delta[\text{Si}/\text{H}]$ (+0.3 dex)	Δ_{sys}
φ Cas	15851.880	0.146	0.067	0.035	-0.018	0.165
	15961.157	0.105	0.085	0.029	-0.030	-0.002	...	0.141
	16133.170	0.139	0.070	0.034	-0.010	...	-0.022	0.161
ν Aql	15851.880	0.048	0.153	0.028	-0.017	0.164
	15961.157	0.054	0.151	0.025	-0.019	-0.015	...	0.164
	16133.170	0.067	0.151	0.046	-0.014	...	-0.088	0.193
HD 190323	15851.880	0.000	0.176	0.066	-0.030	0.190
	15961.157	0.003	0.179	0.057	-0.021	-0.031	...	0.192
	16133.170	0.018	0.175	0.100	-0.026	...	-0.099	0.227
d Dra	15851.880	-0.015	0.196	0.055	-0.011	0.204
	15961.157	-0.002	0.194	0.056	-0.005	-0.121	...	0.235
	16133.170	0.014	0.194	0.081	-0.014	...	-0.149	0.258

Note that, although we fix the Ce abundances of each star to derive the astrophysical gf -values, the Ce abundances are still uncertain within the range of $\lesssim 0.3$ dex (standard deviations, Section 4.1). The Ce abundances scale the resultant gf -values: for example, if the Ce abundance is altered by the standard deviation (Table 2) in the positive direction, the derived gf -values are also affected by the same degree as in the negative direction. Furthermore, it should be noted that the Ce abundances in Luck (2014) as well as the astrophysical gf -values here were derived under the assumption of LTE. Non-LTE treatment may affect the abundances of heavy elements (e.g., Mashonkina et al. 2005), especially in supergiants. This may result in systematic changes in the derived gf -values. Nevertheless, the fact that the derived gf -values are consistent among the samples suggests that the Ce abundance of each star adopted in this work is reasonable. Independent measurements of their stellar parameters may be able to reduce the uncertainties in the astrophysical gf -values, but this is beyond the scope of this work. The uncertainties present here are found not to affect the final results for the kilonova spectra significantly, as discussed in Section 5.

5. Applications to Kilonova Spectra

We apply the derived gf -values of the Ce III lines to calculate kilonova spectra. To calculate synthetic spectra of kilonovae, we use a wavelength-dependent radiative transfer simulation code (Tanaka & Hotokezaka 2013; Tanaka et al. 2014, 2017; Kawaguchi et al. 2018; Tanaka et al. 2018; Kawaguchi et al. 2020). Photon transfer is calculated by the Monte Carlo method. The setup of the simulation is identical to that in Domoto et al. (2022), but we adopt the final astrophysical gf -values of the three Ce III lines derived in Section 4. For more details of the simulation, we refer the reader to Domoto et al. (2022).

Figure 5 shows a comparison between our new synthetic spectra (blue) and the observed spectra of AT2017gfo taken with the Very Large Telescope (VLT; gray) at $t = 1.5, 2.5,$ and 3.5 days after the merger (Pian et al. 2017; Smartt et al. 2017). The observed spectrum at $t = 4.5$ days after the merger taken with the Hubble Space Telescope (HST), which is not affected by telluric absorption, is also shown by a black line (Tanvir et al. 2017). We find that the absorption features around 14500 \AA are caused by the Ce III lines in the new spectra. These

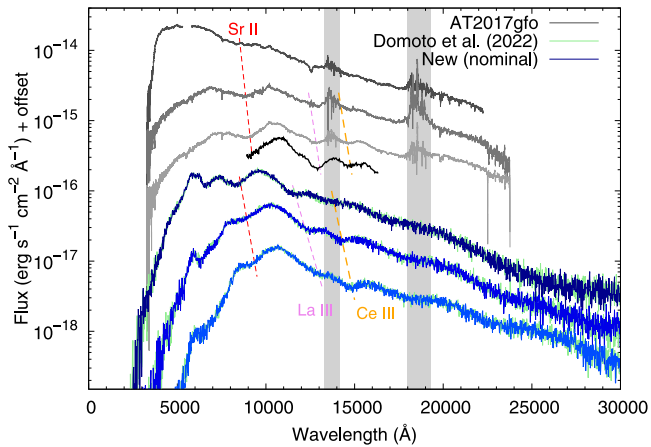


Figure 5. Comparison between the synthetic spectra (blue) and the observed spectra of AT2017gfo taken with the VLT (gray; Pian et al. 2017; Smartt et al. 2017) at $t = 1.5, 2.5,$ and 3.5 days after the merger (dark to light colors). The spectrum taken with the HST at $t = 4.5$ days after the merger (Tanvir et al. 2017) is also shown as a black line. The green curves are the synthetic spectra of Domoto et al. (2022; see their Figure 8). Spectra are vertically shifted for visualization. Gray shaded areas show the regions of strong atmospheric absorption.

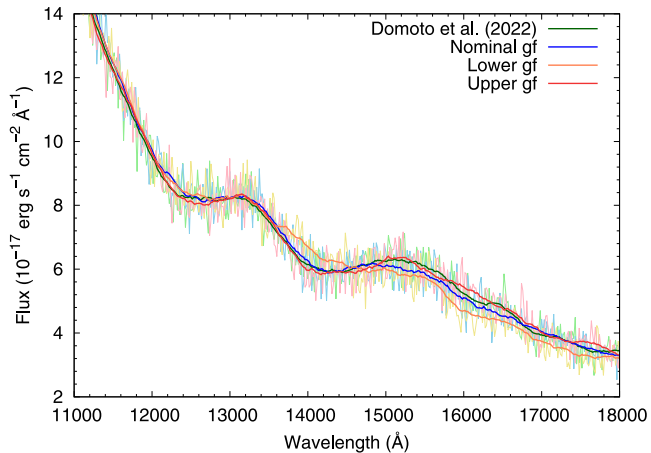


Figure 6. Enlarged view of the synthetic spectrum in the NIR region at $t = 2.5$ days. The blue curve shows the synthetic spectrum using the derived gf -values, and green curve shows that of Domoto et al. (2022). The orange and red curves show the synthetic spectra when using the lower and upper gf -values, which consider the sum of the uncertainties negatively and positively, respectively (see the text). The curves in light colors show the original results, while those in dark colors show smoothed spectra for visualization.

features are blueshifted according to the velocity of the line-forming region at NIR wavelengths, e.g., $v \sim 0.1c$ at $t = 2.5$ days. In fact, the features caused by the Ce III lines in the new synthetic spectra are almost the same as those in Domoto et al. (2022; green), who used the gf -values of Tanaka et al. (2020; see Figure 6 for an enlarged view at $t = 2.5$ days). This is consistent with the observed features in the spectra of AT2017gfo.

To see the effects of the uncertainties in the gf -values on the spectra, we also perform the same simulations by varying the gf -values of the Ce III lines. The orange and red curves in Figure 6 show the results when using the lower and upper gf -values, respectively. Here, for the lower (upper) values, we take the average of the estimated gf -values for each star negatively (positively) shifted by $\sigma_{[\text{Ce}/\text{H}]}$, and then further shift the average by Δ_{sys} negatively (positively). We find that the

changes in fluxes around 14500 \AA are $\sim 10\%$. The absorption features of Ce III are still seen even when using the lower gf -values (orange curves), although the depth of absorption is weakened.

When using the final astrophysical gf -values, the Sobolev optical depths of the Ce III lines for the line-forming region ($\rho \sim 10^{-14} \text{ g cm}^{-3}$ and $T \sim 5000 \text{ K}$; see Domoto et al. 2022) are ~ 4 . The lower gf -values of the Ce III lines are smaller than the nominal values by a factor of ~ 2.7 . Thus, even by adopting the lower gf -values, the Sobolev optical depths of the Ce III lines are still larger than 1. This confirms the identification of Ce in the spectra of AT2017gfo.

The changes in gf -values of the strong lines affect not only absorption but also emission in the spectra. A stronger absorption tends to cause a stronger emission in a P-Cygnit-type line profile. As shown in Figure 6, the increase of the gf -values results in an increase of the flux of the emission component around the rest wavelengths, and vice versa. Note that, for particularly large gf -values (red and green lines), the optical depths of the Ce III lines are large enough that the depth of the absorption is saturated, while the effect in the emission component is still apparent.

6. Summary

We have derived the astrophysical gf -values of the three Ce III lines in the H band using IGRINS spectra of four F-type supergiants. The derived gf -values are systematically lower by about 0.25 dex than those used in Domoto et al. (2022), but they broadly agree with available theoretical calculations within the estimated uncertainties. Using the derived astrophysical gf -values of the Ce III lines, we have performed radiative transfer simulations of kilonovae. We have found that the Ce III lines with the new gf -values produce the absorption features around 14500 \AA in the kilonova spectra, even considering the uncertainties. This supports the identification of Ce in the observed spectra of AT2017gfo (Domoto et al. 2022).

We have also shown that the F-type supergiants with near-solar metallicity show strong absorption of Ce III. To our knowledge, this is the first report of the detection of Ce III lines in the H band for stars with near-solar abundances. As the line blending is not severe in the NIR spectra compared with the optical spectra, those lines may also be useful for stellar spectroscopic studies.

Acknowledgments

We thank R. E. Luck for providing his detailed abundance data, and K. Kawaguchi for valuable discussions. This work used the Immersion Grating Infrared Spectrometer (IGRINS) that was developed under a collaboration between the University of Texas at Austin and the Korea Astronomy and Space Science Institute (KASI) with the financial support of the Mt. Cuba Astronomical Foundation, of the US National Science Foundation under grants AST-1229522 and AST-1702267, of the McDonald Observatory of the University of Texas at Austin, of the Korean GMT Project of KASI, and the Gemini Observatory. Part of the observations in this work were also carried out within the framework of Subaru-Gemini time exchange program which is operated by the National Astronomical Observatory in Japan. We are honored and grateful for the opportunity of observing the Universe from

Maunakea, which has cultural, historical, and natural significance in Hawaii. Some of the numerical simulations presented in this paper were carried out on the Cray XC50 at the Center for Computational Astrophysics, National Astronomical Observatory of Japan. This work was supported by JST FOREST Program (grant No. JPMJFR212Y, JPMJFR2136), NIFS Collaborative Research Program (NIFS22KIIF005), the Grant-in-Aid for JSPS Fellows (22KJ0317), and the Grant-in-Aid for Scientific Research from JSPS (19H00694, 20H00158, 20H05855, 21H04997, 23H00127, 23H04891, 23H04894, and 23H05432). N.D. acknowledges support from the Graduate Program on Physics for the Universe (GP-PU) at Tohoku University.

Appendix Abundance Estimates of Ap Stars as a Test of the Astrophysical gf -values

We assess the validity of our astrophysical gf -values by applying them to the spectra of Ap stars. Ap stars are a kind of CP stars that exhibit extremely high metal abundances. Thanks to the high abundances, Ap stars show clear Ce III absorption lines on which we focus. However, it is also known that they show inconsistent abundances between singly and doubly ionized rare-earth elements (REEs), called the REE anomaly (Ryabchikova et al. 2004; Ryabchikova & Romanovskaya 2017). Even if Ce abundances have been measured from Ce II lines, they do not necessarily represent actual Ce abundances. Therefore, these stars cannot be used to derive the gf -values in Section 4.

Here, we estimate the Ce abundances from Ce III lines (hereafter Ce III abundances) in Ap stars using the derived astrophysical gf -values. We use three Ap stars, HD 101065 (Przybylski's Star), HD 201601 (γ Equ), and HD 24712. These stars have quite different $\log g$ values from the supergiants used to derive the gf -values. Thus, the abundance estimates serve as an independent assessment of the derived gf -values.

The spectrum of HD 101065 was taken with Gemini-South/IGRINS on UT 2022 December 18 in two ABBA sequences, each with an exposure time of 33 s. An A0V star (HIP 55019) was also observed for the telluric standard. Those IGRINS spectra are reduced through the pipeline (Lee et al. 2017), as

described in Section 3.1. The 1D spectra are normalized by continuum fitting.

The spectra of HD 201601 and HD 24712 were taken with the Gemini Near-Infrared Spectrograph (GNIRS; Elias et al. 2006a, 2006b) at the Gemini-North telescope on UT 2022 July 17 and August 18, respectively. We use 110.51 mm^{-1} grating and long camera with a $0''.1$ slit, which gives a spectral resolution of $R \sim 17,800$. The central wavelength is set to $1.6 \mu\text{m}$ to cover the three Ce III lines. HD 201601 and HD 24712 were observed in one and two ABBA sequence(s), each with an exposure time of 60 s, respectively. For the telluric standards, A0V stars (HD 208108 and HD 15130) were also observed. The GNIRS spectra are reduced using the Gemini IRAF package following the standard procedure, which includes flat fielding, sky subtraction, wavelength calibration based on Ar–Xe lamp spectra, and extraction of 1D spectra. The 1D spectra are normalized by continuum fitting. Telluric absorption in the normalized target spectra is corrected by dividing by the normalized spectra of the A0V stars.

Spectra of the three Ap stars around the region of the Ce III lines are shown in Figure 7. For those spectra, we measure the EWs of the three Ce III lines by Gaussian fitting. Then, we perform spectral synthesis as in Section 4 but by changing the Ce abundance and by using the derived gf -values of the Ce III lines. We use the stellar parameters of the Ap stars derived in the literature using optical spectra as summarized in Table 5. Although there are atmospheric parameters derived using more sophisticated models that consider the stratification of elements for all the samples (Shulyak et al. 2009, 2010, 2013), we adopt those derived using 1D atmospheric models (ATLAS) that we use for spectral synthesis. We measure the EWs of the Ce III lines in the model spectra by Gaussian fitting and compare with the EWs in the observed spectra. Comparison is repeated by varying the Ce abundances until the model EWs match with the EWs in the observed spectra.

We show the results of the Ce III abundances estimated using the three Ce III lines in Table 6. It is seen that the line-by-line variation of the abundances is small in each star. This fact demonstrates that the derived gf -values of the Ce III lines are reasonable.

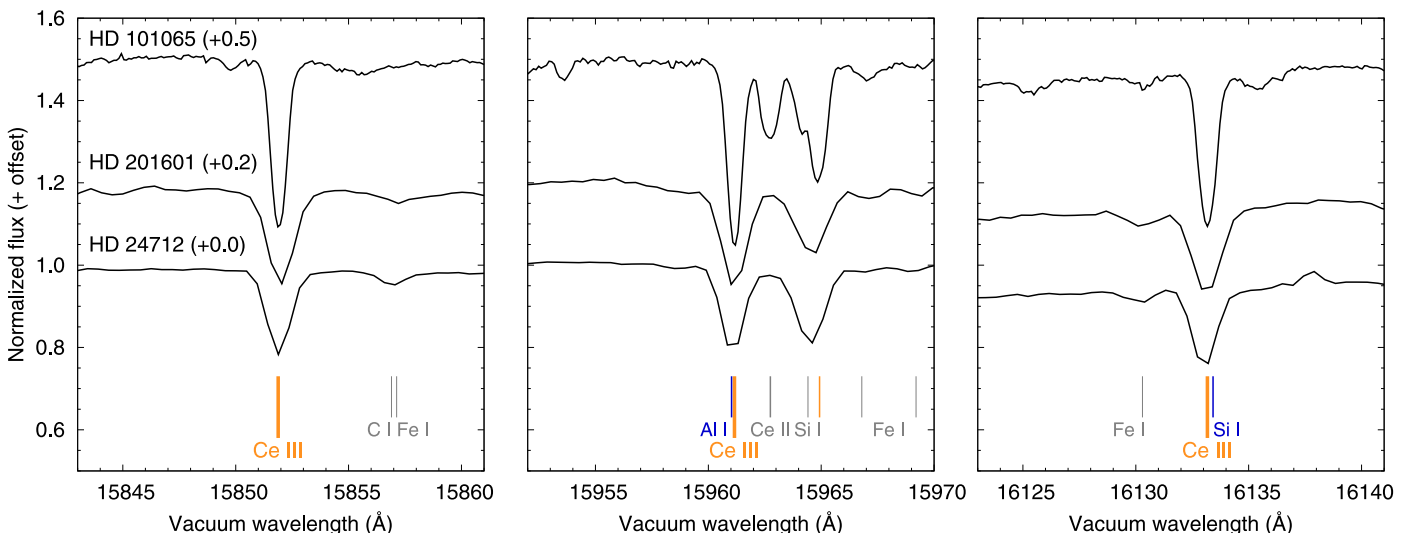


Figure 7. The observed spectra around the Ce III lines of the Ap stars. Absorption lines are labeled as in Figure 1.

Table 5
Adopted Stellar Parameters for the Ap Stars

Star	Model	T_{eff} (K)	$\log g$ (cm s^{-2})	[Fe/H]	ξ (km s^{-1})	$v \sin i$ (km s^{-1})	[Al/H]	[Si/H]	Reference
HD 101065	ATLAS	6600	4.20	-0.72	1.00	3.5	-1.11	0.11	Cowley et al. (2000)
HD 201601	ATLAS	7700	4.20	0.19	2.00	7.0 ^a	0.66	0.11	Ryabchikova et al. (1997a)
HD 24712	ATLAS	7250	4.20	-0.21	1.00	6.6 ^a	0.06	-0.18	Ryabchikova et al. (1997b)

Notes. All $v \sin i$ are smaller than the spectral resolution ($R \sim 45,000$ or $17,800$) and do not affect the results.

^a Adopted from Sikora et al. (2019).

Table 6
Ce Abundances Derived Using Ce III and II Lines in the Ap Stars

[Ce/H]		HD 101065	HD 201601	HD 24712
Ce III	15851.880 Å	4.11	4.09	3.86
	15961.157 Å	4.06	4.04	3.72
	16133.170 Å	4.16	4.26	3.83
	Mean \pm standard error	4.11 \pm 0.03	4.13 \pm 0.07	3.78 \pm 0.03
	Literatures	4.76 ^a	3.46–5.36 ^c	
Ce II		2.93 ^a	1.26 ^d	1.42 ^e
		3.07 ^b		

Notes.

^a Shulyak et al. (2010).

^b Cowley et al. (2000).



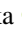





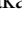
^c Hubrig et al. (2012).

^d Ryabchikova et al. (1997a).

^e Ryabchikova et al. (1997b).

Table 6 also shows the Ce II and III abundances reported in the literature, which confirm a clear REE anomaly. It is worth noting that, although Hubrig et al. (2012) showed that the derived Ce III abundances in HD 201601 deviate by about 2 dex depending on the lines, the abundances derived by using the three Ce III lines here are consistent with each other. Also, this is the first measurement of the Ce III abundance for HD 24712.

ORCID iDs

Nanae Domoto  <https://orcid.org/0000-0002-7415-7954>
 Jae-Joon Lee  <https://orcid.org/0000-0003-0894-7824>
 Masaomi Tanaka  <https://orcid.org/0000-0001-8253-6850>
 Ho-Gyu Lee  <https://orcid.org/0000-0002-3808-7143>
 Wako Aoki  <https://orcid.org/0000-0002-8975-6829>
 Miho N. Ishigaki  <https://orcid.org/0000-0003-4656-0241>
 Shinya Wanajo  <https://orcid.org/0000-0002-4759-7794>
 Daiji Kato  <https://orcid.org/0000-0002-5302-073X>
 Kenta Hotokezaka  <https://orcid.org/0000-0002-2502-3730>

References

Abbott, B. P., Abbott, R., Abbott, T. D., et al. 2017a, *PhRvL*, **119**, 161101
 Abbott, B. P., Abbott, R., Abbott, T. D., et al. 2017b, *ApJL*, **848**, L12
 Abt, H. A., & Morrell, N. I. 1995, *ApJS*, **99**, 135
 Adelman, S. J., Snow, T. P., Wood, E. L., et al. 2001, *MNRAS*, **328**, 1144
 Arcavi, I., Hosseinzadeh, G., Howell, D. A., et al. 2017, *Natur*, **551**, 64
 Asplund, M., Grevesse, N., Sauval, A. J., & Scott, P. 2009, *ARA&A*, **47**, 481
 Biémont, E., Palmeri, P., & Quinet, P. 1999, *Ap&SS*, **269**, 635
 Biémont, E., Quinet, P., & Ryabchikova, T. A. 2002, *MNRAS*, **336**, 1155
 Blanco-Cuaresma, S. 2019, *MNRAS*, **486**, 2075

Blanco-Cuaresma, S., Soubiran, C., Heiter, U., & Jofré, P. 2014, *A&A*, **569**, A111
 Carvajal Gallego, H., Palmeri, P., & Quinet, P. 2021, *MNRAS*, **501**, 1440
 Castelli, F., & Kurucz, R. L. 1994, *A&A*, **281**, 817
 Castelli, F., & Kurucz, R. L. 2003, in IAU Symp. 210, Modelling of Stellar Atmospheres Vol. 210, ed. N. Piskunov, W. W. Weiss, & D. F. Gray (San Francisco, CA: Astronomical Society of the Pacific), **A20**
 Chojnowski, S. D., Hubrig, S., Hesselquist, S., et al. 2019, *ApJL*, **873**, L5
 Cowley, C. R., Ryabchikova, T., Kupka, F., et al. 2000, *MNRAS*, **317**, 299
 Cunha, K., Smith, V. V., Hesselquist, S., et al. 2017, *ApJ*, **844**, 145
 De Smedt, K., Van Winckel, H., Kamath, D., et al. 2016, *A&A*, **587**, A6
 Domoto, N., Tanaka, M., Kato, D., et al. 2022, *ApJ*, **939**, 8
 Domoto, N., Tanaka, M., Wanajo, S., & Kawaguchi, K. 2021, *ApJ*, **913**, 26
 Eichler, D., Livio, M., Piran, T., & Schramm, D. N. 1989, *Natur*, **340**, 126
 Elias, J. H., Joyce, R. R., Liang, M., et al. 2006a, *Proc. SPIE*, **6269**, 62694C
 Elias, J. H., Rodgers, B., Joyce, R. R., et al. 2006b, *Proc. SPIE*, **6269**, 626914
 Evans, P. A., Cenko, S. B., Kennea, J. A., et al. 2017, *Sci*, **358**, 1565
 Freiburghaus, C., Rosswog, S., & Thielemann, F. K. 1999, *ApJL*, **525**, L121
 Ghazaryan, S., Alecian, G., & Hakobyan, A. A. 2018, *MNRAS*, **480**, 2953
 Gillanders, J. H., Smartt, S. J., Sim, S. A., Bauswein, A., & Goriely, S. 2022, *MNRAS*, **515**, 631
 Goriely, S., Bauswein, A., & Janka, H.-T. 2011, *ApJL*, **738**, L32
 Gray, D. F. 2005, *The Observation and Analysis of Stellar Photospheres* (Cambridge: Cambridge Univ. Press)
 Gustafsson, B., Edvardsson, B., Eriksson, K., et al. 2008, *A&A*, **486**, 951
 Hesselquist, S., Shetrone, M., Cunha, K., et al. 2016, *ApJ*, **833**, 81
 Hinkel, N. R., Timmes, F. X., Young, P. A., Pagano, M. D., & Turnbull, M. C. 2014, *AJ*, **148**, 54
 Hinkel, N. R., Young, P. A., Pagano, M. D., et al. 2016, *ApJS*, **226**, 4
 Holtzman, J. A., Hesselquist, S., Shetrone, M., et al. 2018, *AJ*, **156**, 125
 Hony, S., Tielens, A. G. G. M., Waters, L. B. F. M., & de Koter, A. 2003, *A&A*, **402**, 211
 Home, K. 1986, *PASP*, **98**, 609
 Hubrig, S., Castelli, F., González, J. F., et al. 2012, *A&A*, **542**, A31
 Johansson, S., & Litzén, U. 1972, *PhysS*, **6**, 139
 Kasen, D., Metzger, B., Barnes, J., Quataert, E., & Ramirez-Ruiz, E. 2017, *Natur*, **551**, 80
 Kawaguchi, K., Shibata, M., & Tanaka, M. 2018, *ApJL*, **865**, L21
 Kawaguchi, K., Shibata, M., & Tanaka, M. 2020, *ApJ*, **889**, 171
 Korobkin, O., Rosswog, S., Arcones, A., & Winteler, C. 2012, *MNRAS*, **426**, 1940
 Kupka, F., Piskunov, N., Ryabchikova, T. A., Stempels, H. C., & Weiss, W. W. 1999, *A&AS*, **138**, 119
 Lee, J.-J., Gullikson, K., & Kaplan, K. 2017, Igrins/Plp v2.2.0, Zenodo, doi:10.5281/zenodo.845059
 Li, L.-X., & Paczyński, B. 1998, *ApJL*, **507**, L59
 Luck, R. E. 2014, *AJ*, **147**, 137
 Lyubimkov, L. S., Lambert, D. L., Kaminsky, B. M., et al. 2012, *MNRAS*, **427**, 11
 Mace, G., Kim, H., Jaffe, D. T., et al. 2016, *Proc. SPIE*, **9908**, 99080C
 Mace, G., Sokal, K., Lee, J.-J., et al. 2018, *Proc. SPIE*, **10702**, 107020Q
 Majewski, S. R., Schiavon, R. P., Frinchaboy, P. M., et al. 2017, *AJ*, **154**, 94
 Mashonkina, L., Ryabchikova, T., & Ryabtsev, A. 2005, *A&A*, **441**, 309
 Matsunaga, N., Taniguchi, D., Jian, M., et al. 2020, *ApJS*, **246**, 10
 Meléndez, J., & Barbuy, B. 1999, *ApJS*, **124**, 527
 Metzger, B. D., Martínez-Pinedo, G., Darbha, S., et al. 2010, *MNRAS*, **406**, 2650
 Park, C., Jaffe, D. T., Yuk, I.-S., et al. 2014, *Proc. SPIE*, **9147**, 91471D
 Perego, A., Radice, D., & Bernuzzi, S. 2017, *ApJL*, **850**, L37
 Pian, E., D'Avanzo, P., Benetti, S., et al. 2017, *Natur*, **551**, 67

- Piskunov, N. E., Kupka, F., Ryabchikova, T. A., Weiss, W. W., & Jeffery, C. S. 1995, *A&AS*, **112**, 525
- Plez, B., 2012 *Turbospectrum*: Code for spectral synthesis, *Astrophysics Source Code Library*, ascl:[1205.004](#)
- Puķītis, K., Začs, L., & Grankina, A. 2022, *ApJ*, **928**, 29
- Quinet, P., & Palmeri, P. 2020, *Atoms*, **8**, 18
- Rosswog, S., Sollerman, J., Feindt, U., et al. 2018, *A&A*, **615**, A132
- Ryabchikova, T., Nesvacil, N., Weiss, W. W., Kochukhov, O., & Stütz, C. 2004, *A&A*, **423**, 705
- Ryabchikova, T., Piskunov, N., Kurucz, R. L., et al. 2015, *PhyS*, **90**, 054005
- Ryabchikova, T. A., Adelman, S. J., Weiss, W. W., & Kuschnig, R. 1997a, *A&A*, **322**, 234
- Ryabchikova, T. A., Landstreet, J. D., Gelbmann, M. J., et al. 1997b, *A&A*, **327**, 1137
- Ryabchikova, T. A., & Romanovskaya, A. M. 2017, *AstL*, **43**, 252
- Shetrone, M., Bizyaev, D., Lawler, J. E., et al. 2015, *ApJS*, **221**, 24
- Shibata, M., Fujibayashi, S., Hotokezaka, K., et al. 2017, *PhRvD*, **96**, 123012
- Shulyak, D., Ryabchikova, T., Kildiyarova, R., & Kochukhov, O. 2010, *A&A*, **520**, A88
- Shulyak, D., Ryabchikova, T., & Kochukhov, O. 2013, *A&A*, **551**, A14
- Shulyak, D., Ryabchikova, T., Mashonkina, L., & Kochukhov, O. 2009, *A&A*, **499**, 879
- Sikora, J., Wade, G. A., Power, J., & Neiner, C. 2019, *MNRAS*, **483**, 2300
- Smartt, S. J., Chen, T. W., Jerkstrand, A., et al. 2017, *Natur*, **551**, 75
- Smith, V. V., Bizyaev, D., Cunha, K., et al. 2021, *AJ*, **161**, 254
- Soubiran, C., Le Campion, J.-F., Brouillet, N., & Chemin, L. 2016, *A&A*, **591**, A118
- Straizys, V., Cernis, K., & Hayes, D. S. 1985, *Ap&SS*, **112**, 251
- Tanaka, M., Domoto, N., Aoki, W., et al. 2023, *ApJ*, **953**, 17
- Tanaka, M., & Hotokezaka, K. 2013, *ApJ*, **775**, 113
- Tanaka, M., Hotokezaka, K., Kyutoku, K., et al. 2014, *ApJ*, **780**, 31
- Tanaka, M., Kato, D., Gaigalas, G., et al. 2018, *ApJ*, **852**, 109
- Tanaka, M., Kato, D., Gaigalas, G., & Kawaguchi, K. 2020, *MNRAS*, **496**, 1369
- Tanaka, M., Utsumi, Y., Mazzali, P. A., et al. 2017, *PASJ*, **69**, 102
- Tanvir, N. R., Levan, A. J., González-Fernández, C., et al. 2017, *ApJL*, **848**, L27
- Tarumi, Y., Hotokezaka, K., Domoto, N., & Tanaka, M. 2023, arXiv:2302.13061
- Uesugi, A., & Fukuda, I. 1970, *Catalogue of Rotational Velocities of the Stars* (Kyoto: Univ. Kyoto)
- Utsumi, Y., Tanaka, M., Tominaga, N., et al. 2017, *PASJ*, **69**, 101
- Valenti, S., Sand, D. J., Yang, S., et al. 2017, *ApJL*, **848**, L24
- Wanajo, S., Sekiguchi, Y., Nishimura, N., et al. 2014, *ApJL*, **789**, L39
- Watson, D., Hansen, C. J., Selsing, J., et al. 2019, *Natur*, **574**, 497
- Wyart, J.-F., & Palmeri, P. 1998, *PhyS*, **58**, 368